A Triaxial Failure Diagram to predict the forming limit of 3D sheet metal parts subjected to multiaxial stresses

2016 J. Phys.: Conf. Ser. 734 032020

(http://iopscience.iop.org/1742-6596/734/3/032020)

A Triaxial Failure Diagram to predict the forming limit of 3D sheet metal parts subjected to multiaxial stresses

F Rastellini [1,2,*], G Socorro [1], A Forgas [1] and E Oñate [1,2,3]

[1] Quantech ATZ S.A., c/ Gran Capitán 2-4, Barcelona, 08034, Spain.
[2] Centre Internacional de Mètodes Numèrics en Enginyeria (CIMNE).
[3] Universitat Politècnica de Catalunya (UPC), c/ Jordi Girona 3, Barcelona, Spain.

[*] fernando@quantech.es

Abstract: Accurate prediction of failure and forming limits is essential when modelling sheet metal forming processes. Since traditional Forming Limit Curves (FLCs) are not valid for materials subjected to triaxial loading, a new failure criterion is proposed in this paper based on the stress triaxility and the effective plastic strain accumulated during the history of material loading. Formability zones are identified inside the proposed Triaxial Failure Diagram (TFD). FLCs may be mapped into the TFD defining a new Triaxial Failure Curve, or it can be defined by triaxial failure experiments. Several TFD examples are validated and constrasted showing acceptable accuracy in the numerical prediction of forming failure/limit of 3D thick sheet parts.

1. Motivation

Since the classical Forming Limit Curves (FLCs) are only valid for in-plane loading cases, a new approach is required to appropriately render failure curves for materials subjected to multiaxial loads.

The Forming Limit Diagram (FLD) was initially introduced by Keller and Backofen [1] and later improved by Goodwin [2]. Currently, the FLD is widely used in sheet metal forming numerical simulation as a practical and useful criterion to predict the formability limit, based on the in-plane principal strain components.

The fracture loci of metal sheets may be depicted by the Fracture Forming Limit line (FFL) originally proposed by Atkins [3] and by the Shear Fracture Forming Limit line (SFFL). The FFL is related to the reduction in sheet thickness that originates crack opening by tensile stresses (mode I), while the SFFL is related to the distortion that originates crack opening by in-plane shear stresses (mode II).

Whilst the FLC is used for evaluating the formability of the principal strain components under in-plane loading, this criterion is not suitable to predict neither failure nor forming limits when triaxial loads are involved, such in hydro-forming, ironing processes or thick-sheet forming where multiaxial stresses arise.

Due to all these limitations, it is necessary to include the stress triaxiality effect into the formability failure models employed in the numerical simulation of metal forming processes.

2. Formability failure detection under multiaxial loading

Several researches have considered the effect of the stress triaxiality in their fracture failure models. It is worth mentioning the work of Johnson-Cook [4], Lemaitre [5] and Wierzbicki [6].

2.1. Formability failure model including shear fracture

The Modified Mohr-Coulomb (MMC) model was proposed by Bai and Wierzbicki [7] as a ductile fracture model. Subsequently, the same model was successfully applied by Li and Wierzbicki [8]-[9] to predict cracked areas during deep drawing processes.

The MMC fracture model [7]-[10] can predict the ductile fracture damage evolution (D) in terms of the equivalent plastic strain $\bar{\varepsilon}$, the stress triaxiality η and the normalized Lode angle $\bar{\theta}$:

$$D = \int_0^{\varepsilon} \frac{d\bar{\varepsilon}}{f(\eta, \bar{\theta})} \qquad \eta = \frac{\sigma_m}{\bar{\sigma}} \qquad \bar{\theta} = 1 - \frac{6}{\pi}\theta \tag{1}$$

where σ_m is hydrostatic stress and $\bar{\sigma}$ is equivalent stress.

2.2. Proposal of a Triaxial Failure Diagram

An innovative TFD is proposed in this paper including a 3D failure criterion, together with the identification of valid safety zones. The equivalent plastic strain at failure is related in terms of the stress triaxiality. The FLC points are mapped to the new diagram, and extra assumptions are taken to close it for high values of volumetric stresses. The Figure 3 illustrates an example of FLD and TFD safety zones. The names for each safety zone are taken from the industrial jargon currently employed in the FLD for thin sheets: Fail, Thinning, Risk, Safe, Low stretch, Soft compression, Compression, Strong compression.

An internal damage variable should be used for each material point through the simulation aiming to consider the non-linear path evolution and possible changes of the triaxiality values. When fracture damage variable reaches the unity, then the TFC envelope is also reached and failure arises.

2.3. Failure envelope mapping from FFLD to TFD

The failure envelope conversion mapping may be done from the FFLD to TFD space. In the case that complete FFLC (Fracture Failure Limit Curve) is not available; the FLC curve may be used instead.

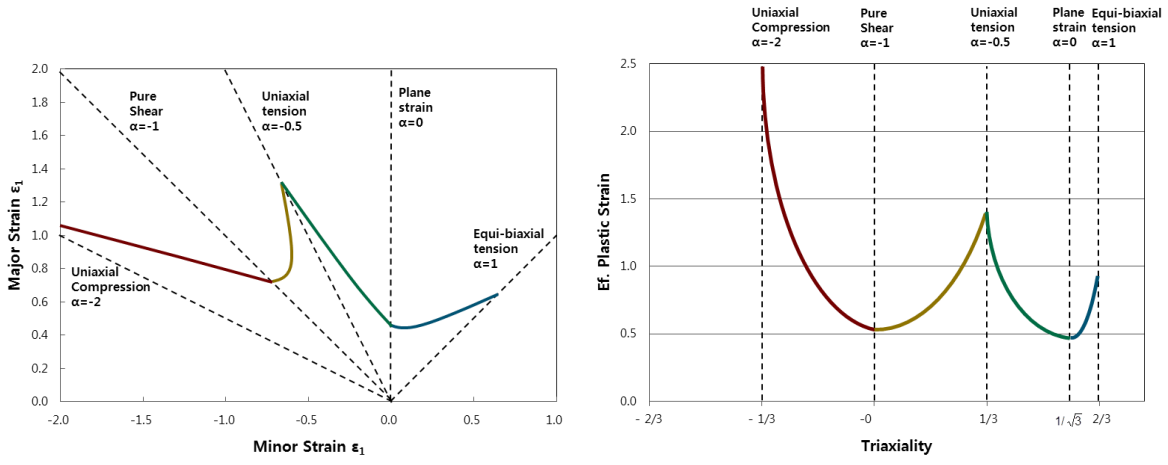

(a) (b)

Figure 1. Conversion mapping from FFLC to TFC. (a) FFLD space. (b) TFD space.

The best would be to perform triaxial testing in the lab, in order to obtain the Triaxial Failure Curve (TFC) envelope. Although, under lack of tests, the FFLC-TFC mapping maybe done as a quite good approximation. The elasto-plastic material parameters are employed. This mapping can only be done

for the plane stress condition; i.e. from triaxiality = –0.66 up to triaxiality = +0.66. Outside this range, some closure lines must also be considered, under lack of additional testing data.

Usually the pure shear failure point is not provided in the FLC curve, so this value may be incorporated as an input parameter from the end-user, aiming to enrich the obtained TFC. Proper consideration of the pure shear failure is essential to capture the crack in many simulation tests.

Even though the mapping is done under plane stress condition, the mapped curve to TFD can be employed in solid elements subjected to multiaxial loading, as a really good failure criterion for 3D solids. The Figure 1 shows the MMC failure model [10] converted from the complete FFLC, including pure shear fracture, into the TFD space.

3. Numerical example validation

A complex industrial process is taken in order to validate the capability of the TFD criterion to predict the failure or the feasibility of metal forming components.

The Stampack^{TM} explicit solver [11] is employed to perform the numerical simulations. Two models are created: the first one employing triangular shell elements [12] with FLC as failure criterion; and the second one employing hexahedral 3D solid elements [13] with TFD failure criterion.

The shear hydro-bending experiment made by Han et al [14] is taken as validation example to execute the numerical simulation analysis, for both shell and 3D solid models.

3.1. Process and material description

The Figure 2 depicts the schematic principle of the shear hydro-bending forming process. During the filling step, the internal pressure is applied. Secondly, the left and right punches provide the proper feeding speed while top and bottom dies are moved down the stroke distance, 40 mm in this example.

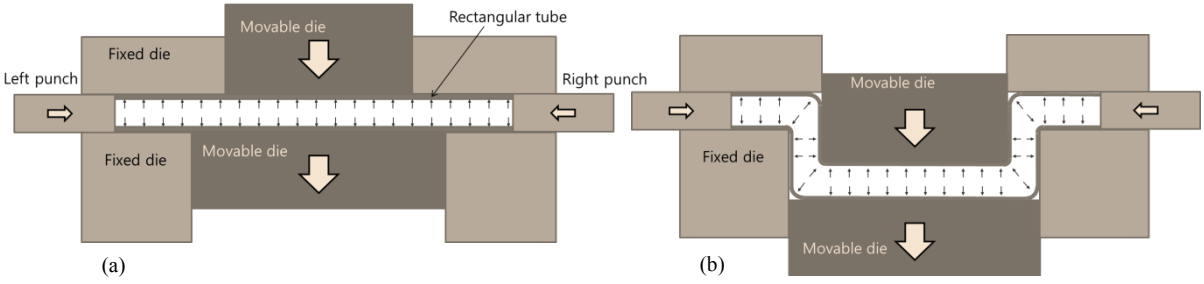

Figure 2. Principle of shear hydro-bending process. (a) Filling stage. (b) Tools movement stage.

Han et al [14] performed the experimental tests under several process conditions: different tool radius, different internal pressures, different axial feeding speeds and different transversal strokes. Nevertheless, in the present analysis, the numerical simulations are studied only for following specific conditions: feeding ratio of 1.2 and internal pressure of 0.6 σ_s. The process defects, such as cracking and wrinkling, of the formed tube do not appear for these parameters [14]. The material employed in the experiment is the 5A02 aluminum alloy, which properties are listed in the Table 1.

Table 1. Material properties of aluminium alloy 5A02.

Properties	Values
Young Modulus	75 GPa
Poisson ratio	0.30
Yield stress (σ_s)	76 MPa
Hardening constant(K)	336.99 Mpa
Hardening exponent(n)	0.254
Tensile strength	184 Mpa
Elongation	22.8 %

The Figure 3 illustrates the FLD and TFD employed during the numerical simulation of the part.

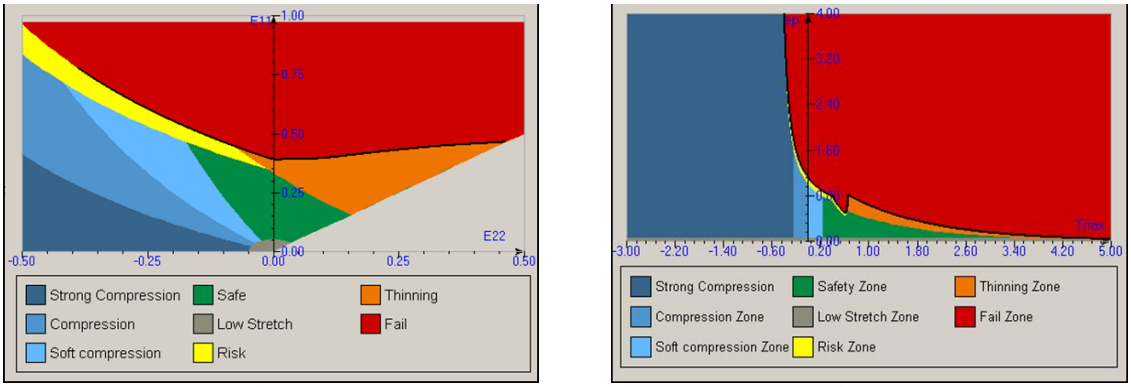

(a) (b)

Figure 3. Safety zones and formability curves for AA 5A04 material. (a) FLD. (b) TFD.

3.2. Comparison with physical part

The numerical simulation results are validated against the physical industrial part produced and published by Han et al [14] and Hong-lae et al [15]. The Figure 4 shows the final shape result obtained by simulation and laboratory. The difference in shape is minimal, but more remarkable aspect is that the part is shown feasible when employing 3D solid elements.

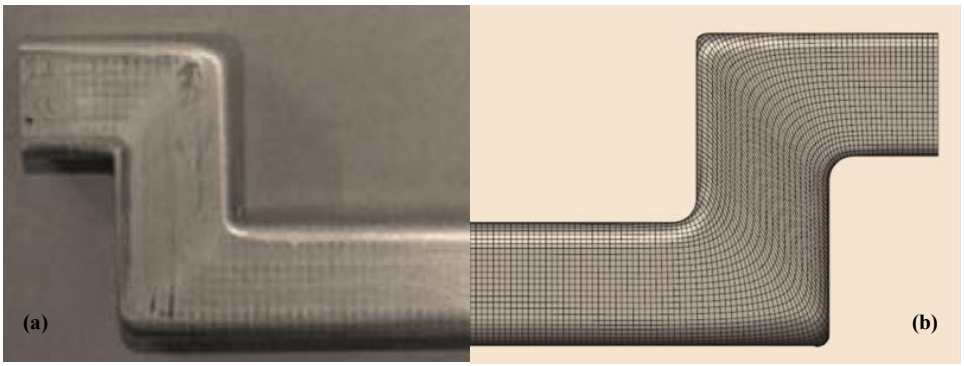

Figure 4. Shear hydro-bending final shape. (a) Physical part (b) Simulation with 3D solid elements.

3.3. Formability analysis given by shell and 3D solid solutions

The Figure 5 shows the postprocess contour fill for the FLD map and safety zones at the end of the forming modelled with shell elements. It can be seen that values over 100% is found in the FLD map meaning that failure is reached for the red colored areas, also marked as failed in safety zone plot.

The Figure 6 displays the contour fill for the TFD map and safety zones obtained with the solid solution, employing MMC triaxial failure. The failure map values below 100% indicate that the onset of fracture was not reached; fact that is also confirmed in TFD safety zone plot.

The Figure 7 provides the formability graph for both shell and solid solutions, where material points are shown to overpass the FLC, while all points remain below the TFC in the 3D solid analysis.

The differences obtained when comparing shell and solid analysis, reflects that FLC is no longer valid as a trusted criterion when multiaxial loads are involved. In contrast with the triaxility approach that provides more reliable results.

The accuracy of the TFD methodology is validated in this analysis of tube hydro-forming process. The result of the 3D solid model is successfully validated against the physical part. Only the new TFD approach is able to confirm the feasibility of this part.

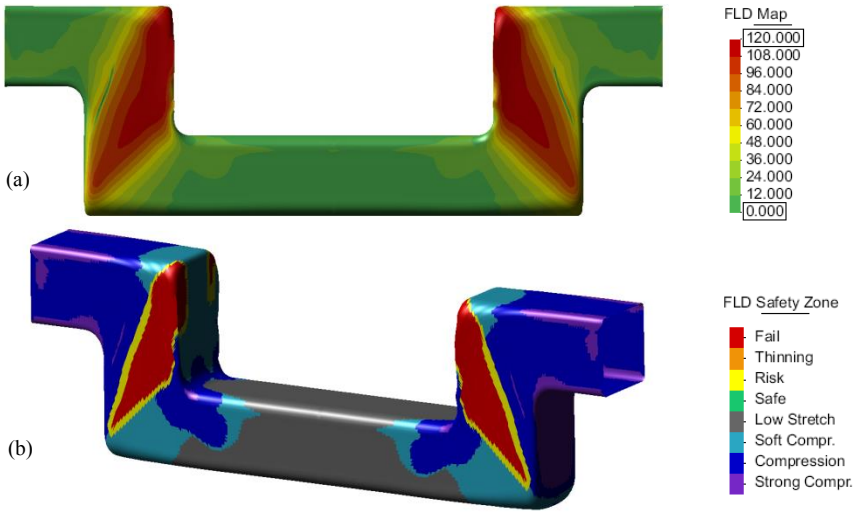

Figure 5. Post-process contour plots from shell elements solution. (a) FLD map. (b) FLD safety zones.

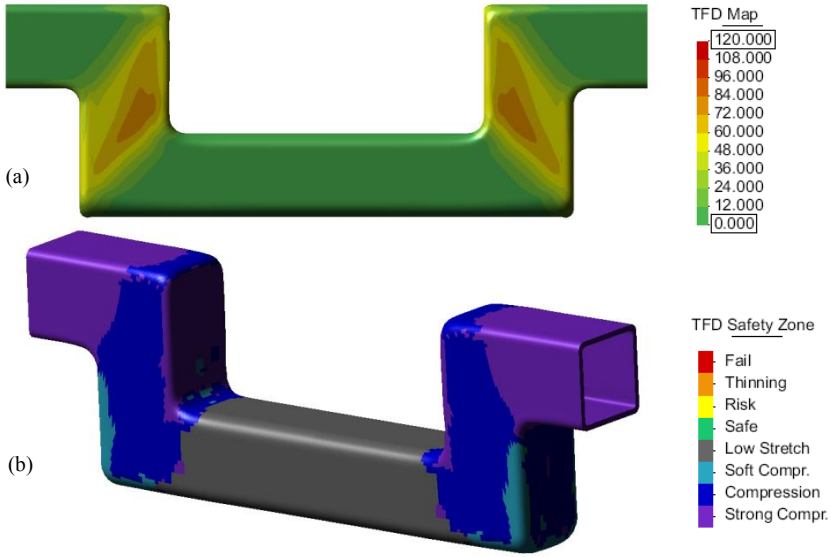

Figure 6. Post-process contour plots from 3D solid elements solution. (a) TFD map. (b) TFD safety zones.

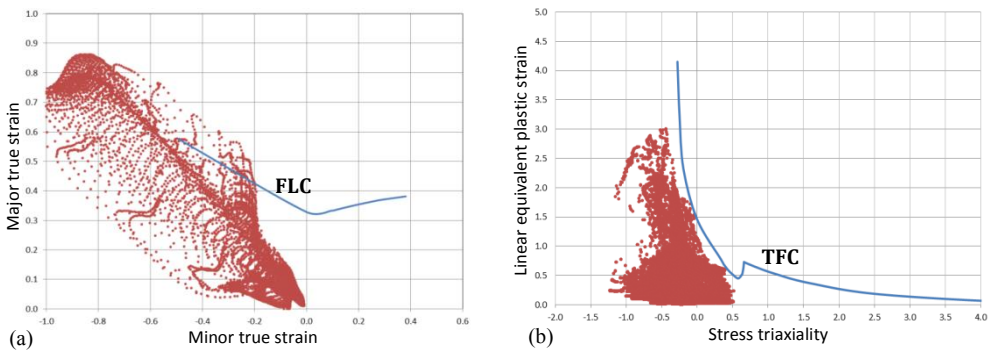

Figure 7. Formability points distribution graph. (a) FLC from shell solution. (b) TFC from solid solution.

4. Concluding remarks

A novel Triaxiality Failure Diagram is proposed as 3D failure criterion, which also allows the identification of valid safety zones. The equivalent plastic strain at failure is related in terms of the stress triaxiality. The FLC points are mapped to the new diagram, and extra assumptions are taken to close it for high values of volumetric stresses.

Numerical simulations of tube hydro-forming are performed employing an explicit solution. Shell and 3D solid models are created to compare both criteria. Results are validated against the physical part produced by the industry. Only the new TFD approach is able to confirm the feasibility of the part. The use of stress-based criteria, like the proposed one, seems to be very convenient for the numerical failure prediction of industrial parts subjected to multiaxial loading.

Acknowledgments

We want to thank Dr. Pablo Vargas who contributed with the results achieved in this research work. We also acknowledge the financial contribution received by the Catalonian government through AGAUR funding granted to Gerardo Socorro.

References

[1] Keeler S, Backofen W. 1963. Plastic instability and fracture in sheets stretched over rigid punches. *ASM TRANS Q* **56** (1), 25–48.
[2] Goodwin G M. 1968. Application of strain analysis to sheet metal forming in the press shop. *SAE paper 680093*.
[3] Atkins A G. 1996. Fracture in forming. *J. Mat. Processing Technology*, **56**, 609-618.
[4] Johnson G R, Cook W H. 1985. Fracture characteristics of three metals subjected to various strains, strain rates, temperatures and pressures. *Engineering Fracture Mechanics*, **21**: 31-48.
[5] Lemaitre J. 1985. A continuous damage mechanics model for ductile fracture. *Journal of Engineering Materials and Technology*, **107**: 83–89.
[6] Wierzbicki T, Bao Y, Lee Y, Bai Y. 2005. Calibration and evaluation of seven fracture models. *International Journal of Mechanical Sciences*, **47**, 719–743.
[7] Bai Y, Wierzbicki T. 2010. Application of extended Mohr-Coulomb criterion to ductile fracture. *International Journal of Fracture* **161** (1), 1–20.
[8] Li Y, Wierzbicki T. 2009. Mesh-size study of ductile fracture by non-local plasticity model. *Proceeding of SEM Annual Conference and Exposition on Experimental and Applied Mechanics*. Paper No. 387.
[9] Li Y, Wierzbicki T. 2010. Prediction of plane strain fracture of AHSS sheets with post-initiation softening. *International Journal of Solids and Structures* **47** (17), 2316–2327.
[10] Li Y, Luo M, Gerlach J, Wierzbicki T. 2010. Prediction of shear-induced fracture in sheet metal forming. *Journal of Materials Processing Technology* **210**, 1858–1869.
[11] STAMPACK^{TM} Reference manual, Version 7.1, Quantech ATZ (www.Stampack.com).
[12] Flores F G, and Oñate E. 2005. Improvements in the membrane behavior of the three node rotation-free BST shell triangle using an assumed strain approach. *Computer Methods in Applied Mechanics and Engineering*, **194**(6), 907−932.
[13] Rastellini F, Díaz G, Forgas A, and Socorro G. 2011. Cutting Strategy for the Numerical Simulation of Multi-Stage Forming of Thick Metal Sheets. *American Institute of Physics Conference Series*. **1383**: 406−412.
[14] Han C, Xu Y, Wang Y, Zang C, Yuan S. 2012. Shear hydro-bending of 5A02 aluminum alloys rectangular tubes. *Transactions of Nonferrous Metals Society of China* **22**, 382−388.
[15] Hong-lae K, Forgas A, Jungsun K, Soontak K and Hotaek K. 2013. Numerical Prediction of the Fracture Using Triaxial Forming Limit in Tube Hydro Forming. *Proceedings of the 6th International Conference on Tube Hydroforming TUBEHYDRO2013*. Jeju, Korea. 243-249.